CONF-900970--1

DE90 015156

TIME DEPENDENT MONTE CARLO CALCULATIONS OF THE ORELA TARGET NEUTRON SPECTRUM

S. N. CRAMER and F. G. PEREY

Oak Ridge National Laboratory
P.O. Box 2008
Oak Ridge, TN 37831-6362

Abstract

The time dependent spectrum of neutrons in the water-moderated Oak Ridge Electron Linear Accelerator (ORELA) target has been calculated using a modified version of the MORSE multi-group Monte Carlo code with an analytic hydrogen scattering model. Distributions of effective neutron distance traversed in the target are estimated with a time and energy dependent algorithm from the leakage normal to the target face. These data are used in the resonance shape analyses of time-of-flight cross section measurements to account for the experimental resolution function. The 20 MeV–10 eV energy range is adequately represented in the MORSE code by the 174 group VITAMIN-E cross section library with a P_5 expansion. An approximate representation of the ORELA positron source facility, recently installed near the target, has been included in the calculations to determine any perturbations the positron source might create in the computed neutron distributions from the target. A series of coupled Monte Carlo calculations was performed from the target to the positron source and back to the target using a next-event estimation surface source for each step. The principal effect of the positron source was found to be an increase in the distance for the lower energy neutron spectra, producing no real change in the distributions where the ORELA source is utilized for experiments. Different configurations for the target were investigated in order to simulate the placement of a shadow bar in the neutron beam. These beam configurations included neutrons escaping from: (1) the central tantalum plates only, (2) the entire target with the tantalum plates blocked out, and (3) only a small area from the water. Comparisons of the current data with previous calculations having a less detailed model of the tantalum plates have been satisfactory.

Research sponsored by the Office of Fusion Energy, U.S. Department of Energy, under contract DE-AC05-84OR21400 with Martin Marietta Energy Systems, Inc.

INTRODUCTION

Time-dependent Monte Carlo calculations have been performed to determine the characteristics of neutrons escaping from the Oak Ridge Electron Linear Accelerator (ORELA) target. From these computed data the delay-time distributions (resolution function) can be estimated for use in the resonance shape analysis of time-of-flight neutron cross section measurements at the ORELA facility. A cut-away drawing of the water-cooled and water-moderated target is shown in Fig. 1. The electron beam creates a bremsstrahlung photon source in the tantalum plates which produces the neutron source from photoneutron reactions in the tantalum. The energy calibration for time-of-flight cross section measurements using this neutron source must have not only the distance from the target face to the detection location, but also an additional effective flight distance for the neutron time delay before escape from the target. This delay time distance distribution is computed from a time- and energy-dependent Monte Carlo calculation with the independent time variable being redefined as a distance equal to the elapsed time of the neutron from birth to escape in the target multiplied by the neutron velocity at escape. The computed histogram distributions are fit to convenient analytical forms for subsequent use in the cross section measurement analysis. In the sections to follow the details of the Monte Carlo calculations will be presented along with some representative results and comparisons with similar studies. The details of the treatment of the calculated data and its use in cross section resonance shape analysis will be presented at a later time. Although the actual distance traveled for each neutron escaping the target could be used in accumulating the desired distributions, the distance variable is used in analyses such as these so that the effective target delay time distance is correlated to the neutron escape energy. In an earlier study (Coceva, et al 1983), similar delay-time distributions were calculated on an ORELA target model slightly different from that now in use. The tantalum plates were given only an approximate representation, and no neutrons were allowed to escape from this central area, simulating a shadow bar to block out direct neutrons from the tantalum. In the current study a detailed spatial and energy model of the tantalum plates has been employed. In addition to the shadow bar configuration described above, distributions were computed for neutrons escaping from the tantalum target only with the water blocked out and also from only a small square area in the water region. An approximate representation of the ORELA positron source facility, recently installed near the target, was included in some of the calculations to determine any perturbation the positron source might create in the computed distributions from the ORELA target. A series of coupled calculations was performed from the target to the positron facility and back to the target using a next-event estimation surface source for each step. For a calculation of the desired distributions on a system such as the ORELA target, the use of a continuous-energy Monte Carlo code would seem most appropriate. However, due to project time and budgetary constraints and the non-standard nature of the required computed output and the history file creation for the positron source coupling, a modified version of the ORNL in-house MORSE multi-group Monte Carlo code was used (Cramer, 1985). A large, fine-group cross section set adequately represented all materials except for the hydrogen in water, for which an analytic model was developed. All calculations were run on the Radiation Shielding Information Center (RSIC) Data General Eclipse MV/4000 mini-computer.

TARGET CALCULATIONAL MODEL

The ORELA target was modeled as shown in the vertical and horizontal cuts in Fig. 2. Except for the shaded tantalum plate assembly, the interior of the target is water. The inlet and outlet cooling water pipes, internal baffles, water channels, and other details were omitted. The thicknesses of the tantalum plates and the neutron production fractions are shown in Table 1, numbering from the left with plate #10 closest to the electron beam entrance. It is assumed that this production is uniform in each plate along the direction of the incident electron beam except for plate #10 where a linear distribution, starting from zero at the leading edge, was used. The spatial distribution across the width and height of each plate was selected from a centered radial Gaussian distribution with a standard deviation of 1 cm. Neutrons were emitted isotropically in the tantalum at time zero. The

group structure by log-log interpolation for the source energy group selection over the 10.68 ev–19.64 MeV energy range of the calculation. The neutron cross section data used in the calculations were taken from the 174 group VITAMIN-E library (Weisbin, et al, 1979) and generated with a P_5 expansion. A separate oxygen-only mixture with the same density as for oxygen in water was

created in order to determine the struck nuclide for a neutron collision in water. Data generated for 300°K were used since the cooling water circulating throughout the target and position source keeps the average temperature close to this value.

Table 1. Tantalum plate data

Plate Number	Thickness (cm) *	Neutron Production Fraction (Alsmiller and Moran, 1967)
1	0.6756	0.0183
2	0.4648	0.0344
3	0.3505	0.0561
4	0.2667	0.0848
5	0.2184	0.1117
6	0.1930	0.1346
7	0.1803	0.1523
8	0.1778	0.1638
9	0.2032	0.1638
10	0.3023	0.0802

* Water gap of 0.0965 cm between all plates.

Table 2. Neutron source energy spectrum (Alsmiller et al., 1970)

Energy (eV)	Relative Yield
2.0(+7) *	6.0(-7)
8.2(+6)	1.0(-5)
3.0(+6)	3.0(-4)
1.8(+6)	1.0(-3)
1.0(+6)	1.8(-3)
7.0(+5)	2.5(-3)
2.0(+5)	2.5(-3)
1.0(+4)	1.2(-3)
1.0(+3)	1.0(-3)

* Read as $2.0 \times 10^{+7}$.

The MORSE code was run using the standard non-escape and non-absorption features. Neutron histories were terminated by the Russian roulette option or when the neutron energy was degraded below 10.68 eV. The non-escape option increases the running time per history over the default method, but for small, high-leakage systems such as the ORELA target the overall efficiency of the calculation is increased by its use. The collision routine COLISN was modified to randomly determine the struck nuclide for a neutron collision in water. This is done by comparing for each pre-collision energy group the total cross sections of the water and extra oxygen media obtained by calls to the NSIGTA routine. For an oxygen collision in water, the calculation proceeds in the normal multigroup mode. If a hydrogen collision is chosen, a discrete pre-collision energy E_i is randomly selected from the pre-collision energy group uniformly across the group. For isotropic scattering in the center-of-mass system the post-collision energy E_o is

$$E_o = E_i \frac{(A^2+2\eta A+1)}{(A+1)^2} , \tag{1}$$

where η is the center-of-mass scattering angle cosine, $-1 \le \eta \le 1$, and A is the nuclide-to-neutron mass ratio. The laboratory scattering angle cosine for isotropic scattering is related to the center-of-mass angle as

$$\mu = \frac{1+A\eta}{\sqrt{A^2+2A\eta+1}} . \tag{2}$$

The scattering probability for hydrogen in the center-of-mass system is $p(\eta) = 1/2$. It is assumed here that $A = 1$ (i.e., that the neutron and hydrogen nuclide have the same mass, the actual difference being less than one percent). With these values and Eq. 2, the scattering function relationship $p(\mu)d\mu = p(\eta)d\eta$ gives $p(\mu) = 2\mu$, $0 \le \mu \le 1$. The laboratory scattering angle cosine for a neutron scatter with hydrogen is then selected for the continuation of the random walk as the square root of a uniform random number on the unit interval. The outgoing energy from Eq. 1 becomes $E_o = E_i\mu^2$, and the post-collision energy group for the continuation of the multigroup calculation is that group whose upper and lower limits bracket E_o.

Following each collision and source event in the random walk, an estimate of the time- and energy-dependent neutron leakage was made with modified versions of the standard RELCOL and SDATA routines. Estimation trajectories for neutron escape were chosen to be perpendicular to the side of the target; i.e., the calculated results simulate the effect of a parallel beam of neutrons in a flight path rotated 90° from the electron beam axis. (This calculational procedure differs from that of the earlier study where the results were averaged within a 30° cone relative to the target side.) Due to the symmetry of the entire system, an estimate was made to each side of the target following each event with the final results being halved. The point flux estimator was modified by eliminating the $1/r^2$ term, giving the leakage as neutrons/sec/steradian. For hydrogen the scattering distribution given above was used, which limits the estimation to one face only. At the event site, μ is defined between the incident neutron direction and that to the closest point on the target face. The coupling of the continuous and multigroup energy modes for the estimation process is the same as that outlined for the random walk in selecting and incident discrete energy and setting the post-collision estimation energy group. Estimates were made, or rejected, depending on the position of the event site relative to the target side in order to simulate use of a shadow bar for the three configurations of data collection (see Introduction). The time of the neutron escape estimate was determined from the time since birth at the event site plus the estimation trajectory traverse time. For the conversion to the effective distance variable, this total time was multiplied by the neutron velocity corresponding to the mid-energy of the estimation post-collision energy group. The results were collected into 52 distance intervals of 0.25 cm width followed by 10 additional intervals of 2.0 cm for a total range of 0 to 33 cm. The first 52 intervals (13 cm) were used for the ORELA target calculations alone, and the additional intervals were used to study the effect of the positron source facility on

the effective distance distributions in the target.

POSITRON SOURCE CALCULATION

A positron source facility has recently been installed close to the target as shown in Fig. 3. This water-cooled facility consists of aluminum-clad tungsten plates. Positrons are produced via pair-production in tungsten from photons escaping from the target. There is no neutron production in the positron source facility, but neutrons leaking from the target can scatter from the source facility back into the target and create a late-time (and large effective distance) perturbation in the distribution of escaping neutrons. The positron extraction apparatus, being much farther from the target than indicated in the schematic, was excluded from the model. To estimate the effect of the source facility, coupled calculations were performed from the target to the source and back to the target, followed by a final target calculation as described in the previous section. Modified versions of the MORSE history file reading and writing modules were used to create the necessary neutron source from one step of the calculation to the next. The modifications consisted of creating surface sources for each step from next-event estimation to a surface during the random walk of the previous step. For the purpose of determining the effect on the target delay-time distributions the positron source was given a spherical representation conserving the masses of the actual facility. The model consists of a central 2.23-cm radius tungsten sphere, an intermediate 3.66-cm radius water shell, and an outer 6.00 cm aluminum spherical shell. The calculational model of the coupled system is shown in Fig. 4. The target representation is the same as the lower view in Fig. 2. The centers A and B of the two volumes are co-planar as shown, 24.53 cm apart and are on the axis of the electron beam coming from the right. The outer spherical radius is R_s, and the cylinder has a radius of R_c and a height of $2t$. The point P_1 represents a source or collision event as described in the previous section from which a leakage estimate to the target side is made. Also at P_1 a current estimate (neutrons/sec) is made to the point P_{2s} on the surface of the sphere from the flux point estimator with the $1/r^2$ term replaced with $\Delta\Omega$, the solid angle, in steradians, subtended at P_1 by the spherical volume. From the spherical surface exposed to the target (all points P_{2s}), a random walk is begun into the positron source. At collision events P_2 shown a distance h below the beam axis in Fig. 4, the same estimator is used to place a source at points P_{3s} on both the curved and flat surfaces of the cylindrical target, including the extended notched area. Here the $\Delta\Omega$ is the solid angle subtended at P_2 by the cylindrical target. The final step of the calculation is the same as for the target alone in the previous section, with the source now defined by the points P_{3s} on the cylindrical surface exposed to the sphere. It is due to the time elapsed for these multiply transferred neutrons, as compared to those escaping directly from the target that the ten extra bins (see the previous section) have been added for the calculation of the effective distance distributions.

The solid angle $\Delta\Omega$, a random estimation trajectory, and surface source sites P_{2s} or P_{3s} must be determined at each event site P_1 and P_2. In general, the points P_1 and P_2 will neither lie in the vertical or horizontal planes as defined by the volume centers A and B. The distance r_1 is from P_1 to the spherical center, and r_2 is the horizontal distance from P_2 to the target cylindrical axis. The procedure for a spherical volume is a much-utilized method in Monte Carlo applications. The spherical solid angle as seen at P_1 is

$$\Delta\Omega = 2\pi\left(1-\sqrt{1-(R_s/r_1)^2}\right) . \qquad (3)$$

A random estimation scattering angle cosine within $\Delta\Omega$ is, for a uniform random number RN on the unit interval, $\cos\omega = 1 - RN\,(\Delta\Omega / 2\pi)$. With a random azimuthal angle, the direction cosines of the estimation trajectory and the surface intercept can be determined using the same rotational equations as for the direction components following a random walk collision. Many approximate methods exist for the determination of the solid angle of a cylinder relative to an external point, and an exact method using elliptical integrals has been developed (Cramer, 1981). However, it has been found that from both a coding and computational aspect, the commonly-used rejection technique is the most efficient method when the point does not closely approach the cylindrical surface. In the rejection technique, the body in question (here a cylinder) is circumscribed by another body for which

properly normalizing the estimation. The most common circumscribing body is a sphere, but this method is inefficient here due to the disk shape of the target. Instead, a solid angle is calculated as $\Delta\Omega = \Delta\gamma\Delta\phi$ where γ and ϕ represent a polar angle cosine

and an azimuthal angle, respectively, as defined from a coordinate system with its origin at P_2 and a vertical axis parallel to the target cylindrical axis. These polar angle cosine limits for the configuration as shown in Fig. 4 ($h > \ell$) are defined as

$$\gamma_{1,2} = \frac{+(h \pm \ell)}{\sqrt{(r_2 \mp R_c)^2 + (h \pm \ell)^2}} \quad . \tag{4}$$

When P_2 is in the same relative position a distance h above the electron beam axis, Eq. 4 is altered by reversing all algebraic signs except the central sign under the radical. When only the curved surface of the target is exposed to P_2, then $h \leq \ell$ and the same conditions hold except that only the negative sign is used in the first term under the radical. A third case, not applicable here, exists when $r_2 \leq R_c$ (i.e., only the flat circular end of the cylinder is exposed to the point in question). The $\Delta\gamma$ in $\Delta\Omega$ is defined as $\gamma_1 - \gamma_2$ from Eq. 4, and cos ω for the random trajectory is chosen uniformly between these two limits. Unlike the spherical volume, the azimuthal angle limits for a cylinder (not shown in Fig. 4) must be computed for each P_2 (except for the third case).

$$\phi_{1,2} = \pm \cos \sqrt{1 - (R_c / r_2)^2} \quad . \tag{5}$$

The $\Delta\phi$ in $\Delta\Omega$ is $\phi_1 - \phi_2$, and a random trajectory azimuthal angle is selected uniformly between these limits. The estimator is evaluated using cos ω and $\Delta\Omega$, creating the surface source P_3 for the final step of the coupled calculation. The random trajectory-cylindrical volume intercept (or miss) can be evaluated analytically as for the corresponding spherical case, or use may be made of the standard ray-tracing method in the code. The intercept efficiency for this third-step calculation was greater than 95% for the source-target geometry, and some idea of such an efficiency should be obtained prior to the use of any solid angle calculation using a rejection method. In the method using the exact cylindrical solid angle, the limits of the polar angle cosine are dependent on the independently chosen azimuthal angle, and the exact $\Delta\Omega$ for a cylinder is much more difficult to determine than $\Delta\gamma\Delta\mu$.

PRESENTATION OF CALCULATED RESULTS

The calculated output of the MORSE code for this study is the time- and energy-dependent neutron leakage perpendicular to the face of the ORELA target. The time variable multiplied with the neutron velocity at escape gives an effective distance, and the results are collected into intervals of distance instead of time for various energy intervals. Typical sets of leakage output are shown in Fig. 5 for various energy intervals in the configuration with the tantalum plate target blocked out, each indicated energy being contained within a different interval. Here, the effective distance variable has been collected for each escaping neutron to form a probability curve versus distance. The curve is normalized such that the area under the analytic fit (the smooth line) is unity. Only one set of calculated data points is shown, and these data at the mid-point of each 0.25-cm interval represent the Monte Carlo results averaged over the interval. The error bars represent the statistical uncertainty in terms of plus or minus one standard deviation of the average value. Each smooth curve is the least-square fit of the data to a chi-square distribution. In Fig. 5 the results are for the target only. In Fig. 6 similar results for the target are plotted (upper data, now on a log scale) as well as those results (lower data) collected for neutrons which have scattered to the positron source, back into the target, and then escaped perpendicular to the target face. Beyond 13 cm the results are collected in 2 cm intervals. The area under the backscattered curve is less than one per cent of that for the direct data, and this ratio is typical of all energy intervals. Fig. 7 gives comparisons between the current evaluations without the positron source and the earlier results. The leakage spectra are virtually identical within the context of the different energy intervals. In Figs. 8-10, data for the different configurations in the current study are compared. The small square configuration is for the entire target blocked out except for leakage from a square of 6.45 cm^2 in the water centered 2.54 cm directly above (or below) the tantalum plates. The difference in the two water-only leakage spectra in Fig. 8 is almost constant with energy and is due to the difference in the surface areas of the two configurations (a factor of 21). In Fig. 9, the means

The variances of the effective distance, the second moment of data used to compute the mean, is shown in Fig. 10. Although Fig. 7 shows very good agreement with the earlier results for the neutron leakage, comparisons of the other data (not shown with the current results in Figs. 8 and 9) shows that for the current calculations the means are approximately 10% smaller and the variances

20% larger than the previous calculations for the entire energy range. These differences can be attributed to combinations of various differences in the two calculations: large differences in the tantalum plate model (direct estimation from the tantalum plates being blocked out in both cases), small differences in overall geometric modeling, the estimation process (perpendicular leakage versus a conical spread), and the cross section data evaluations and library creation and utilization.

SUMMARY AND CONCLUSIONS

A calculational analysis of the ORELA target has been conducted to determine the characteristics of the neutron leakage perpendicular to the target faces for three configurations involving the water and the tantalum plates. Results compiled include the leakage spectrum, the probability distribution of effective delay-time distances as a function of energy, the distribution in energy of the average distance traveled in the target before escape, and the variance of this distance distribution. Comparison of this data for the configuration of the water with the tantalum plates blocked out with that computed from an earlier, less detailed target model gives good agreement. It can be seen from Fig. 5 that the effective moderation distance increases with increasing energy. The mean for these and other energy intervals not shown are plotted as the top curve for the water mean distances in Fig. 9. The energy dependent curves in Fig. 5 are all normalized to unit area, whereas the top curve in Fig. 8 gives the absolute energy dependent leakage spectrum per source neutron. From the figures presented it is seen that the histogram data can be fitted to analytic forms. The effective distance data is used to redefine the target-detector distance for use in the resonance shape analysis of time-of-flight neutron cross section measurements at the ORELA facility. The MORSE multi-group Monte Carlo code was used in the analysis, and it was modified to include an analytic treatment for hydrogen scatter. A second set of calculations included a spherical model of the ORELA positron source facility in order to determine if any backscatter effects from the facility could perturb the neutron leakage and effective distance distributions for the target alone. A three step calculation from the target assembly to the positron facility and back to the target was completed using next-event surface estimation techniques to create the source for steps two and three. Solid angle determinations for both spherical and cylindrical bodies subtended at a point were used in the estimation. From data such as that presented in Fig. 8 it can be seen that the backscatter from the positron facility extends the effective distance distribution beyond that for the target alone. However, the magnitudes of these extended distance distributions are of such low value, as compared to the direct effect of the target, that is has been concluded that the positron facility has no effect on the normal operation of any time-of-flight measurement programs at the ORELA facility.

REFERENCES

1. R. G. Alsmiller and H. S. Moran (1967), *Nucl. Inst. Meth.*, 48: 109.
2. R. G. Alsmiller *et al.* (1970), *Nucl. Sci. Eng.*, 40: 365.
3. C. Coceva *et al.* (1983), *Nucl. Inst. Meth.*, 211: 459.
4. S. N. Cramer (1981), *Nucl. Sci. Eng.*, 79: 417.
5. S. N. Cramer (1985), *Applications Guide to the MORSE Monte Carlo Code*, ORNL/TM-9355.
6. C. R. Weisbin, *et al.* (1979), *VITAMIN-E: An ENDF/B-V Multigroup Cross-Section Library*, ORNL-5505 or RSIC DLC-113C.

DISCLAIMER

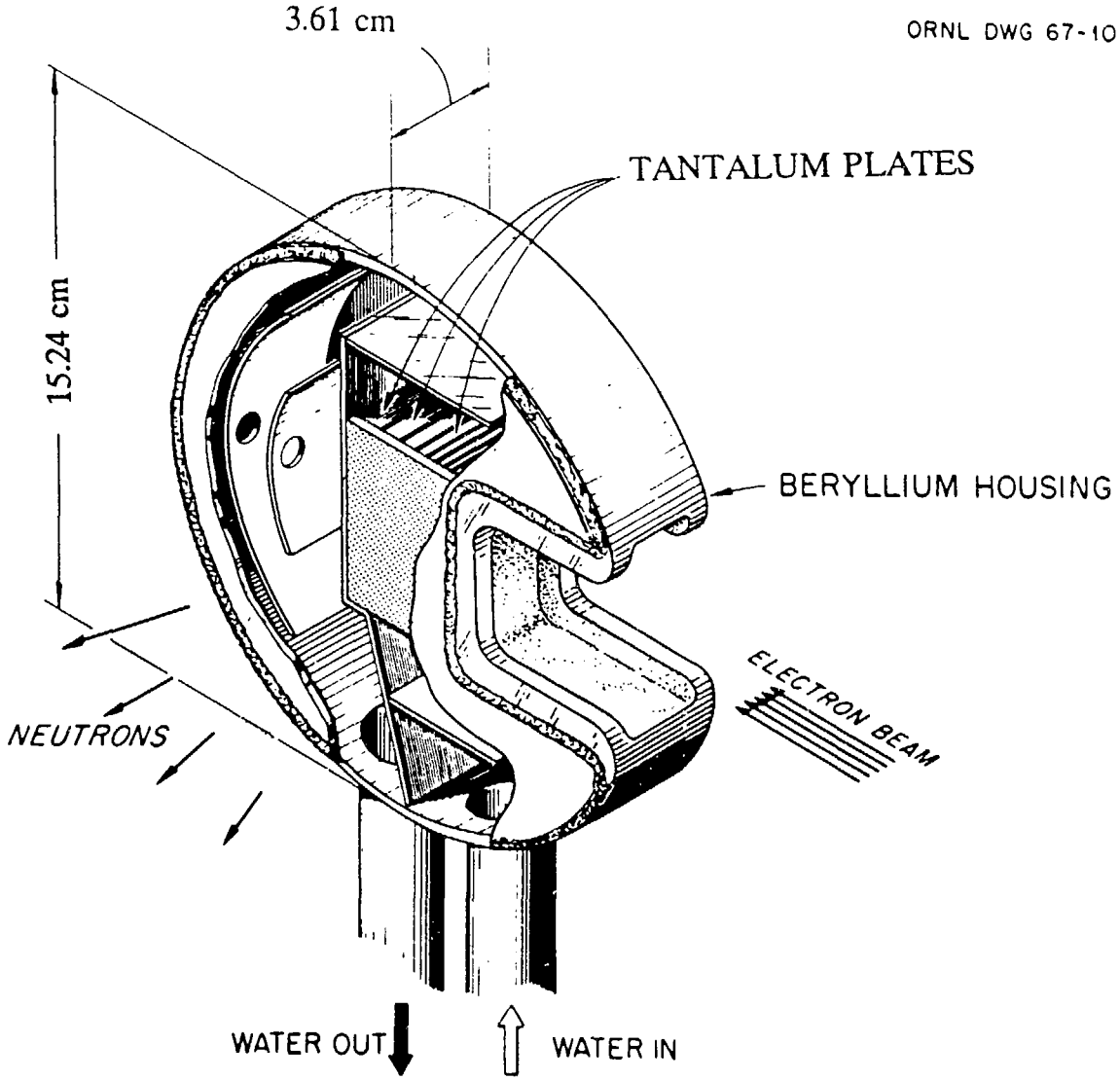

Fig.1 ORELA target assembly

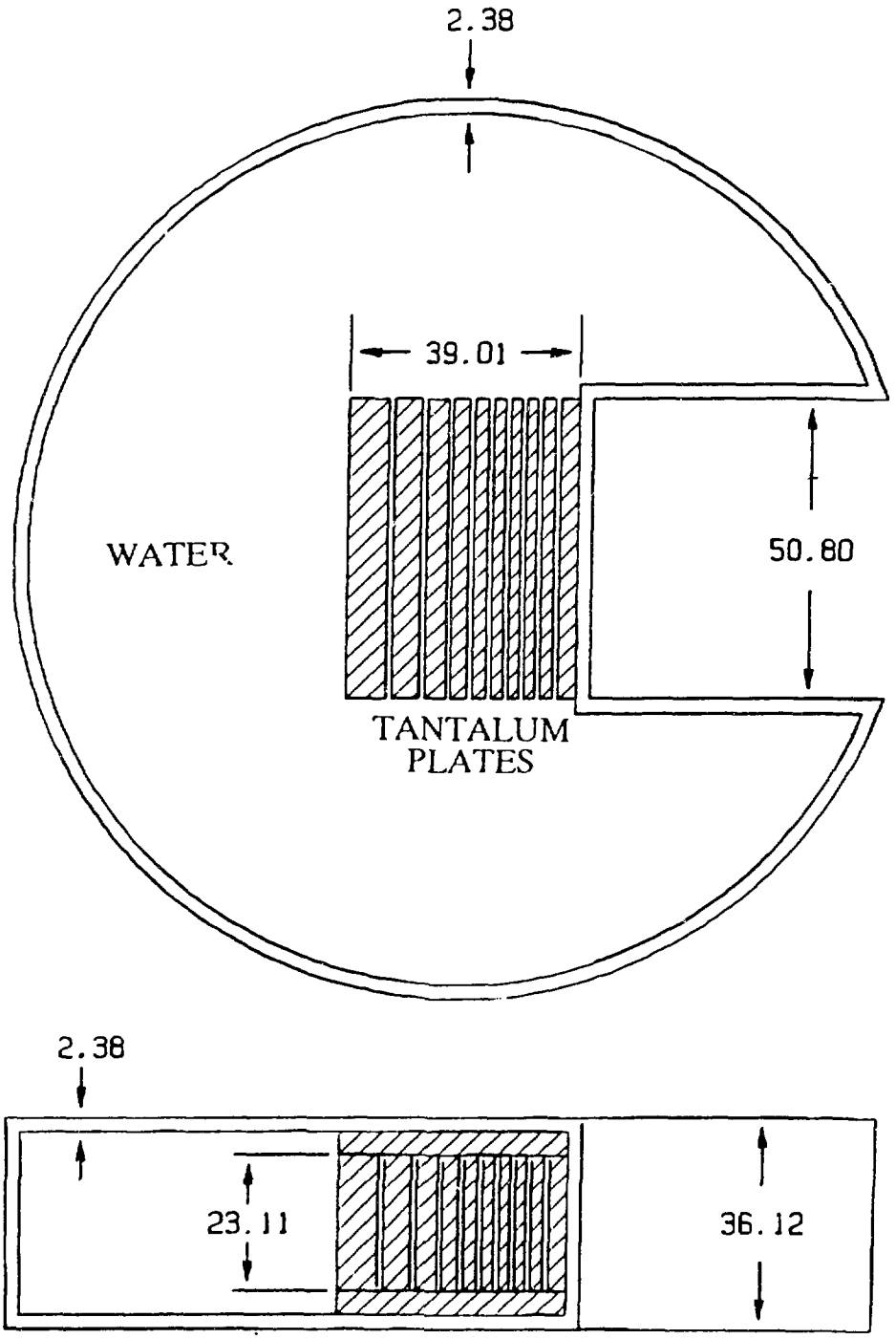

Fig. 2 Model of the 15.24 cm diameter ORELA target (dimensions given in mm)

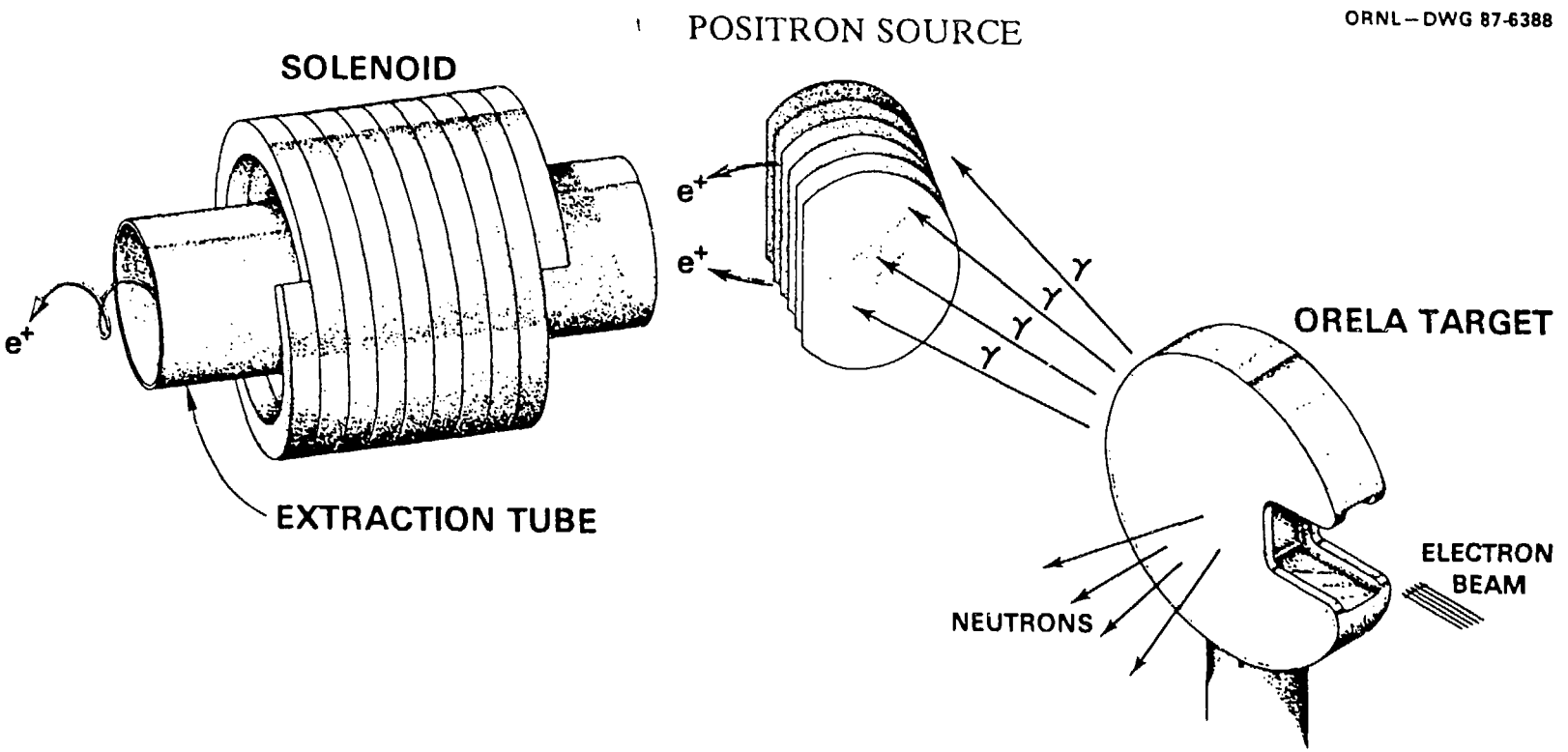

Fig. 3 ORELA positron source facility

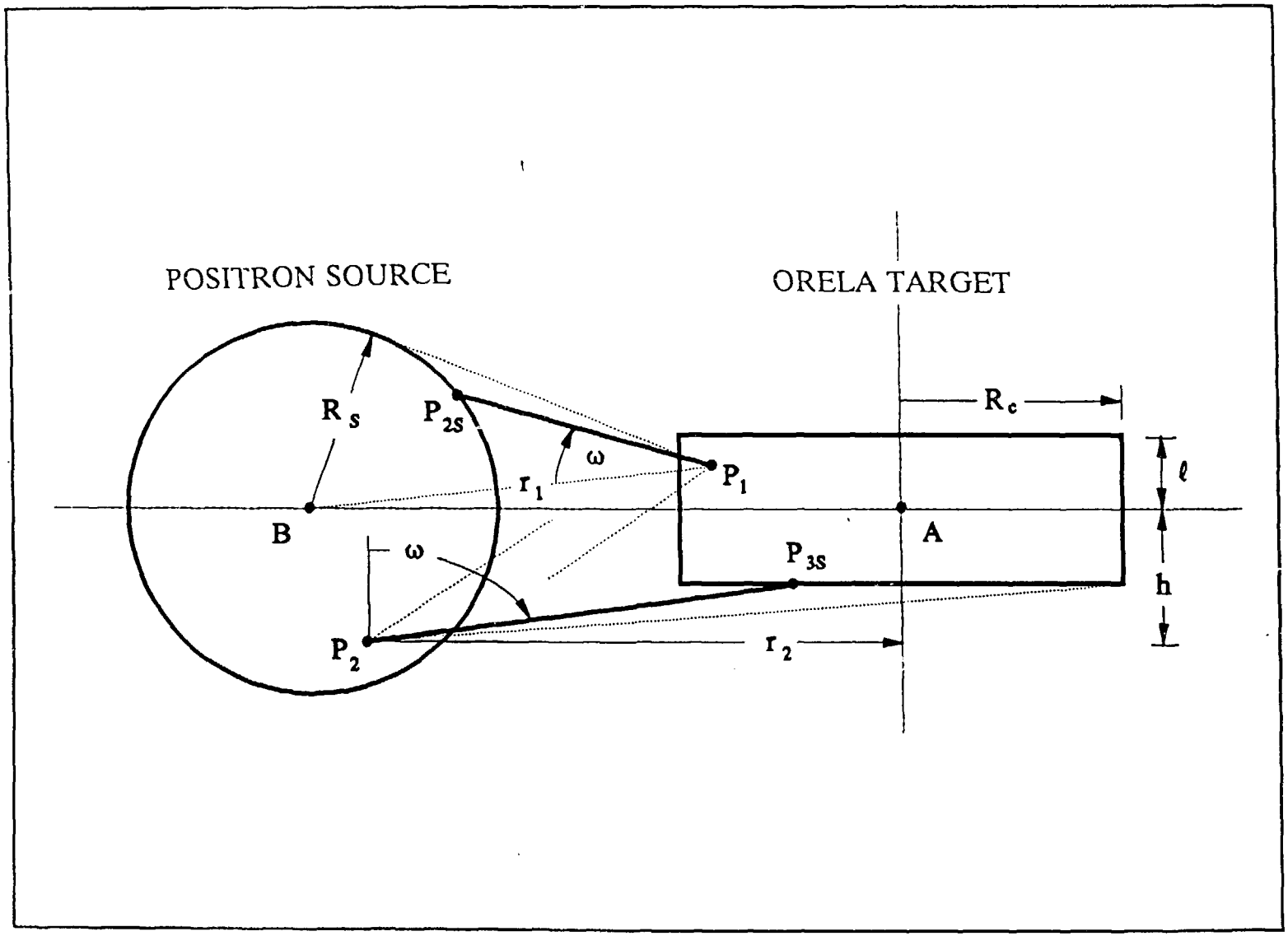

Fig. 4 Spherical positron source model and cylindrical target

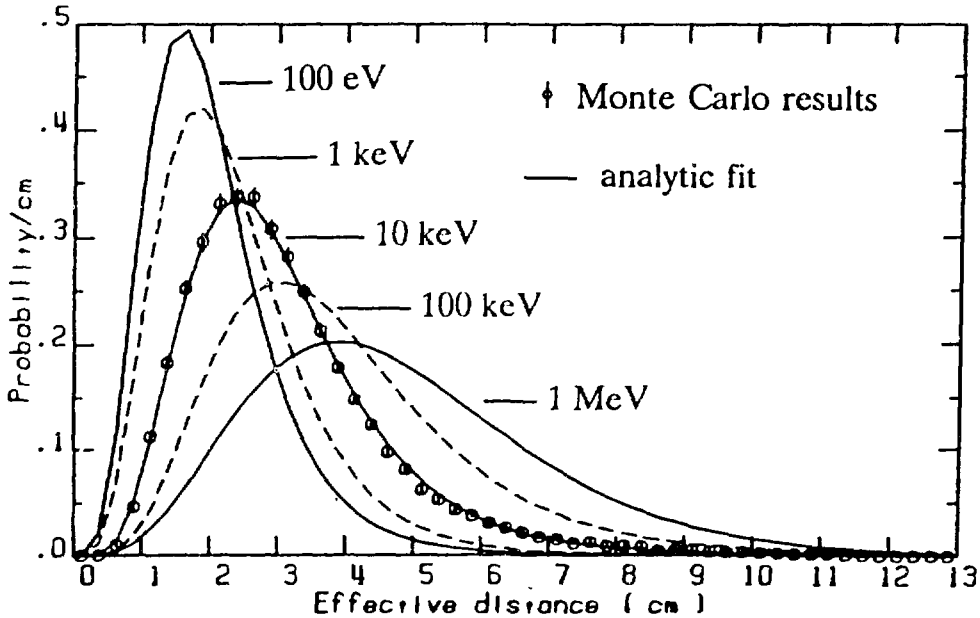

Fig. 5 Neutron effective distance distributions from the water with the tantalum plates blocked out

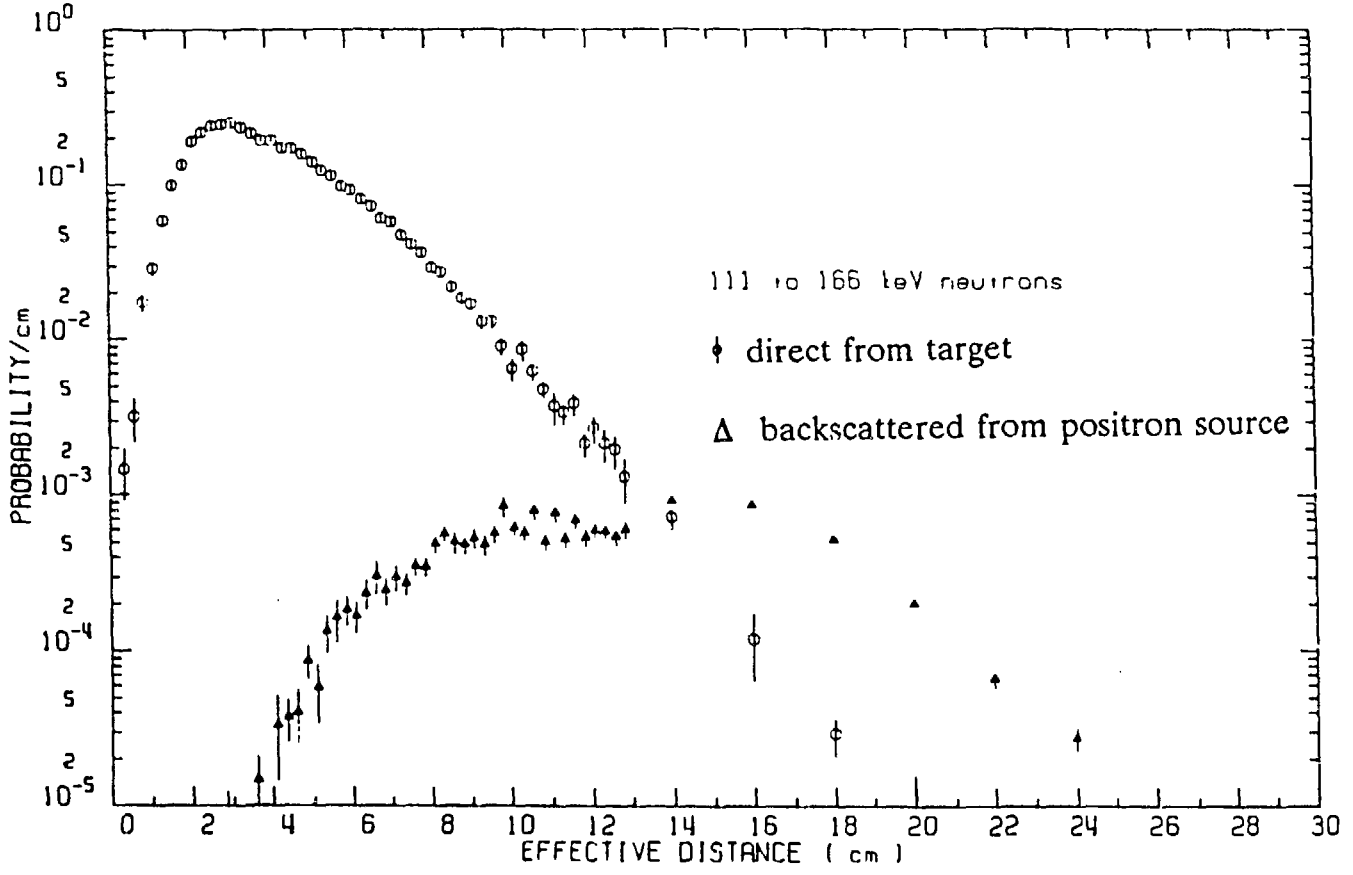

Fig. 6 Direct and backscattered effective distance distributions from the ORELA target

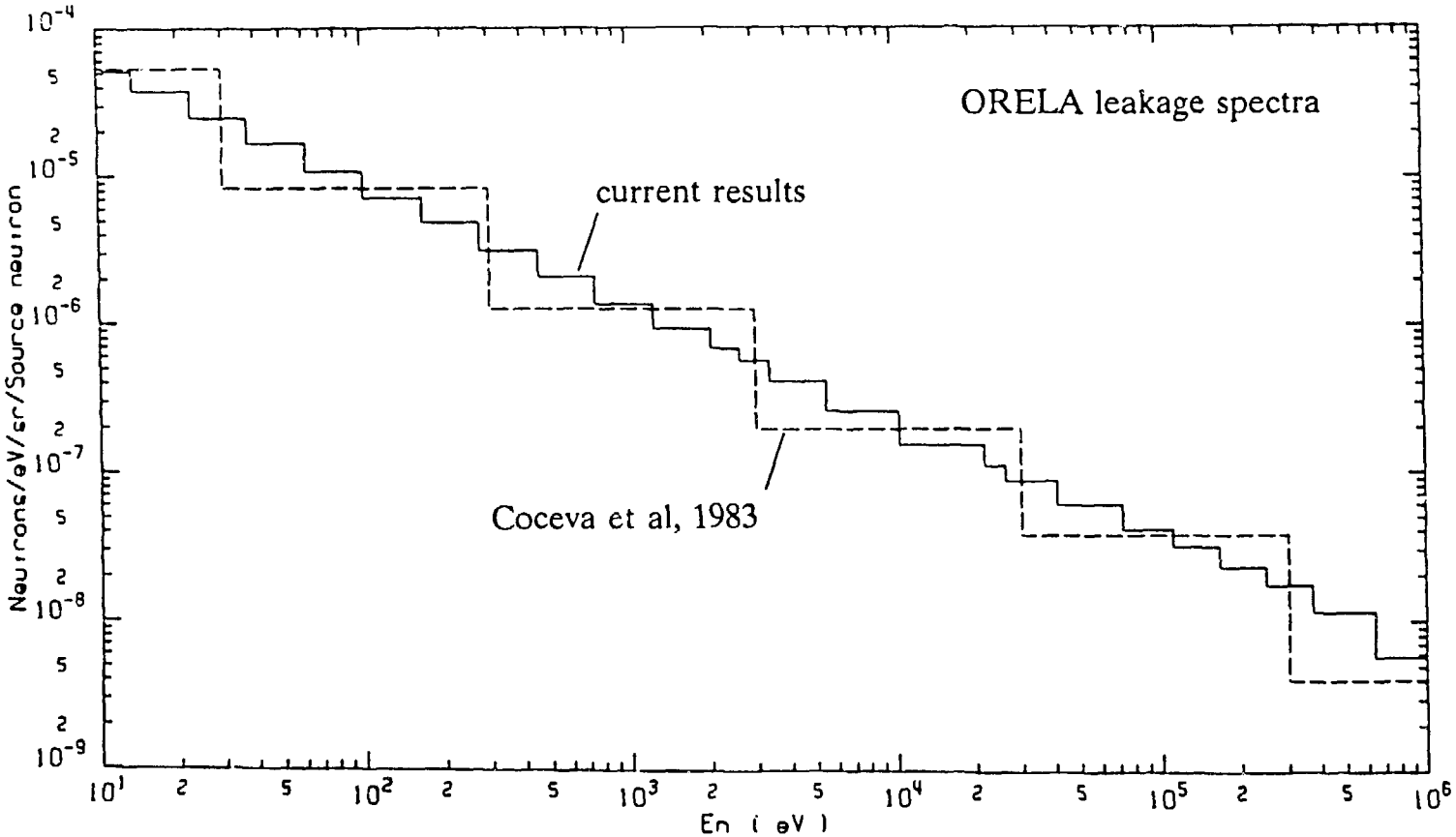

Fig. 7 Comparison of the ORELA target neutron leakage spectrum with the tantalum plates blocked out

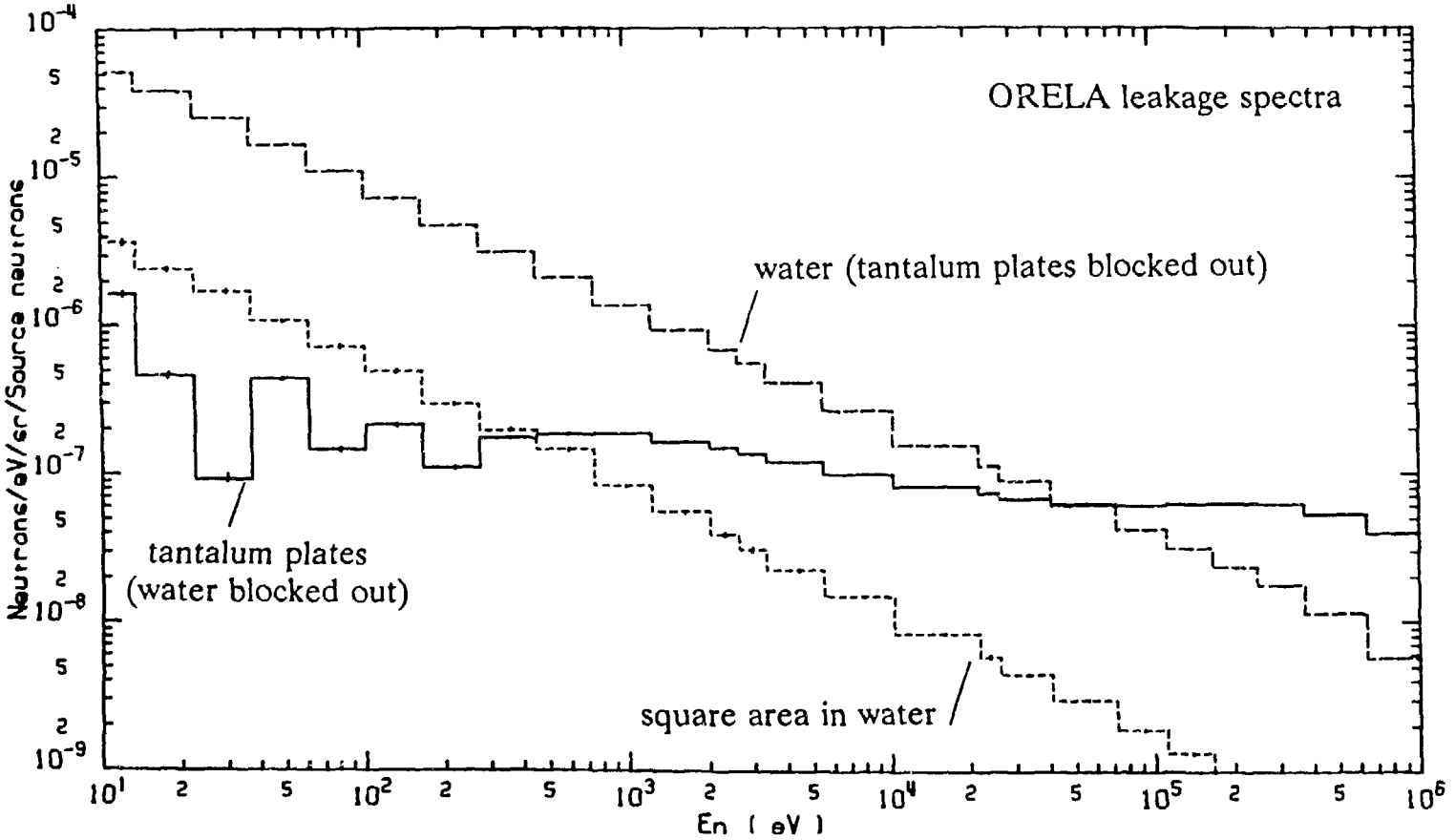

Fig. 8 Neutron leakage spectra for the three ORELA target configurations

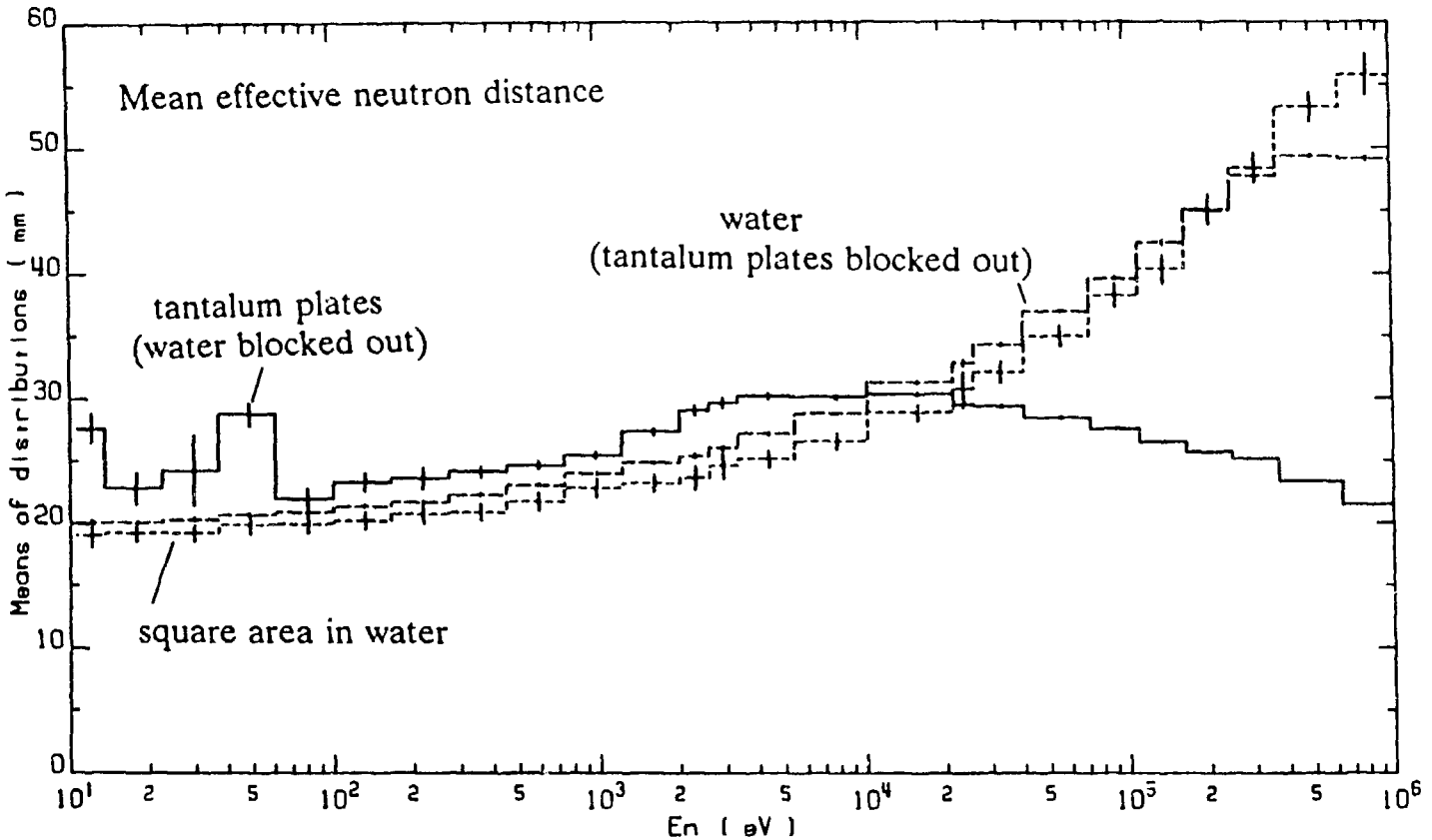

Fig. 9 Mean effective neutron distances for the three ORELA target leakage configurations

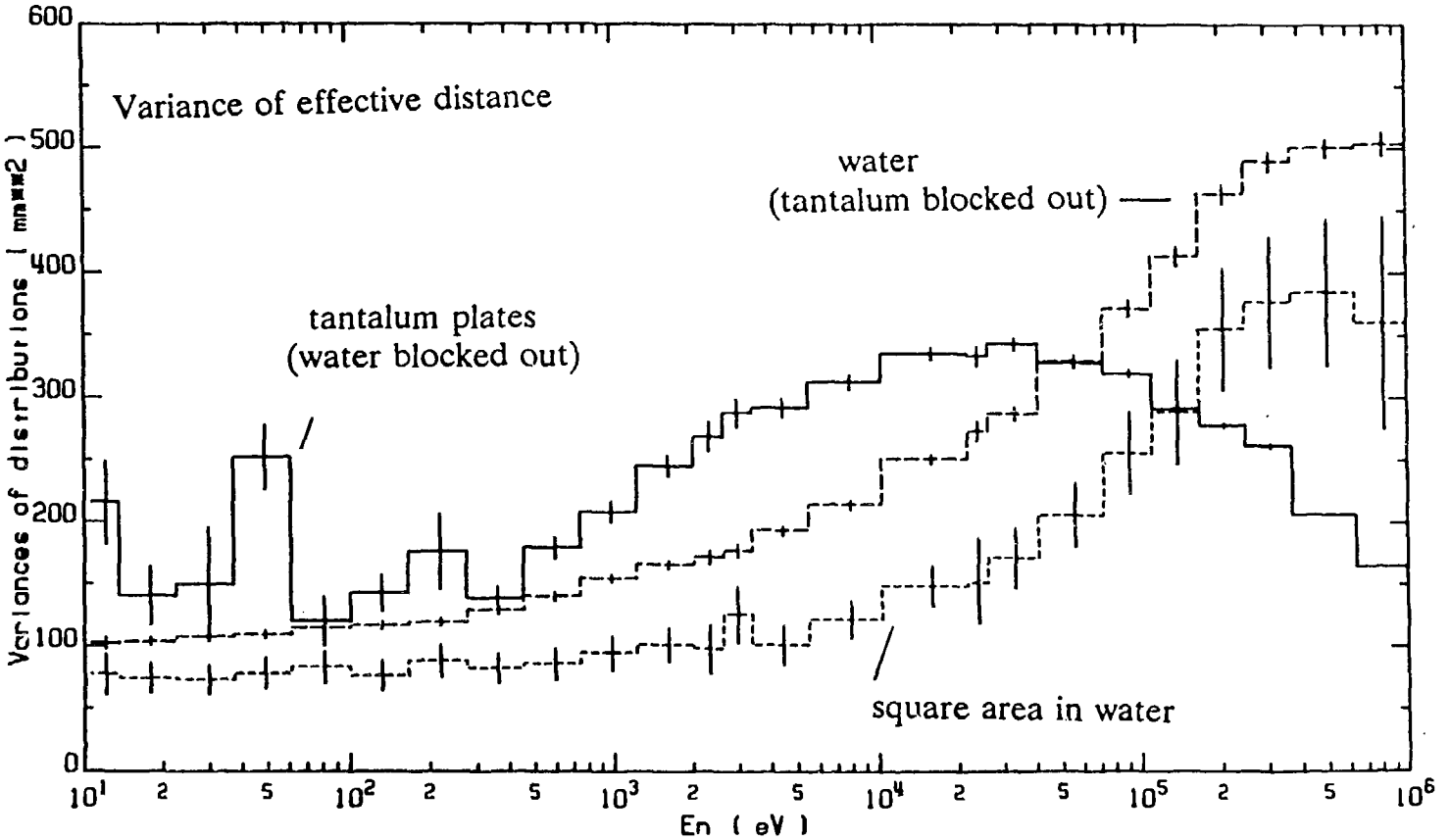

Fig. 10 Variance of the mean effective neutron distances for the three ORELA target leakage configurations